Macromolecules

pubs.acs.org/Macromolecules Article

Leveraging Impurities in Macromonomers from Direct-Growth Polymerizations to Produce Supersoft Bottlebrush Networks with Tunable Mechanical Properties

Yutong Liu, Henry L. Cater, Anthony J. Arrowood, Gabriel E. Sanoja,* and Zachariah A. Page*

Cite This: *Macromolecules* 2024, 57, 6522−6530 Read Online

ACCESS | Metrics & More | Article Recommendations | Supporting Information

ABSTRACT: Bottlebrush polymers are coveted for their supersoft, tissue-like properties. Accordingly, several approaches have emerged to create these materials, yet synthetic challenges remain regarding the number of iterative reactions required to prepare precursors and the cocreation of difficult-to-remove impurities, such as unfunctionalized or bis-functionalized macromonomers (MMs). In this work, we develop a tandem photoiniferter and ring-opening metathesis polymerization method to furnish poly(*n*-butyl acrylate) bottlebrush polymers and networks without the requirement for MM postfunctionalization or the addition of further cross-linking agents. Systematic optimization of polymerization conditions enabled the preparation of ultrahigh-molecular-weight bottlebrush polymers (∼1000 kDa) with narrow dispersity (∼1.2) along with solvent-free elastomers having moduli akin to those of supersoft biological tissues (∼10 kPa). Mechanical properties of the networks were easily tailored by controlling the conversion of photoiniferter polymerization due to its correlation with the amount of in situ cross-linker formed. This report provides a streamlined approach to generate bottlebrush polymers while simultaneously providing structure−property relationships that will inform their preparation and utility in biomedical applications, such as tissue engineering and adhesives.

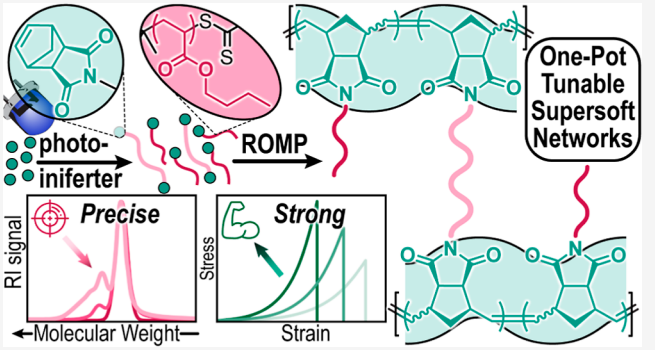

INTRODUCTION

Bottlebrush polymers are a class of macromolecules where densely grafted side chains lead to an extension of the linear backbone and a reduction in entanglement density.[1,2] This combination imbues bottlebrushes with unique bulk mechanical properties that emulate biological tissues, such as skin.[3] Particularly, supersoft moduli (<100 kPa) in the absence of solvent become possible. Consequently, the bottlebrush architecture has been incorporated into a variety of materials such as elastomers,[3−5] photonic crystals,[6,7] photoresists,[8] and pressure-sensitive adhesives.[9] Systematic studies have shown that changes to the bottlebrush architecture (e.g., side-chain length and -density and backbone length) have a dramatic influence on the mechanical properties.[10−12] In particular, high-molecular-weight polymers are attractive as they tend to improve strength and toughness while, in the case of block copolymers, providing access to unique optical properties (e.g., structural color[7,13−15]). Despite this, a comprehensive examination that connects different synthetic strategies of macromonomers (MMs)—macromolecules functionalized with a polymerizable handle [e.g., (meth)acrylate or norbornene]—to corresponding bottlebrush polymer architectures and mechanical properties is lacking. This gap in knowledge necessitates a careful look at MM synthesis to identify structure−property relationships that will inform future design, synthesis, and implementation of bottlebrush polymers.

The most common strategy to synthesize bottlebrush polymers is "grafting-through," which represents the direct polymerization of a MM.[1] In contrast to "grafting-through," "grafting-from" or "grafting-to" strategies often do not provide reliable access to a high density of side chains.[16,17] Ring-opening metathesis polymerization (ROMP) of norbornene-containing MMs represents the most popular "grafting-through" approach, owing to its rapid initiation when employing Grubbs' third generation catalyst (G3), along with its high reactivity capable of overcoming the large thermodynamic energy barrier to propagating MMs with intrinsic steric bulk. Furthermore, ROMP provides excellent control over both molecular weight, dispersity (*Đ*), and chain-end fidelity, which facilitates the synthesis of well-defined, high-molecular-

Received: June 18, 2024
Accepted: July 2, 2024
Published: July 12, 2024

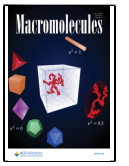

https://doi.org/10.1021/acs.macromol.4c01419
Macromolecules 2024, 57, 6522−6530

weight bottlebrush (block) (co)polymers. However, to achieve high-molecular-weight polymers requires ultrapure MMs, which remain challenging to synthesize.[1,18−24]

Norbornene-functionalized MMs are conventionally synthesized via controlled radical polymerizations of (meth)acrylics or styrenics or ring opening polymerization of lactones, epoxides, or siloxanes.[18,25−28] The norbornene at the polymer chain-end is either installed from the outset (i.e., direct-growth from a functionalized initiator) or via postpolymerization modification (i.e., growth-then-coupling).[19−21] The major impurities that result from direct-growth for controlled radical polymerizations are α,ω-bisnorbornenyl (bis-Nb) MMs and ROMP reactive ω-alkene MMs from termination by combination and disproportionation, respectively. Moreover, radical addition to norbornene followed by chain propagation can also occur.[21] Alternatively, growth-then-coupling introduces an additional synthetic step that can result in nonquantitative monomer incorporation at the chain-end, especially for high-molecular-weight MMs (e.g., >5 kDa) or formation of bifunctional MMs for the case of diol impurities commonly present in commercial poly(ethylene glycol) and poly(dimethylsiloxane) precursors.[26] As a result, bi- and nonfunctionalized MM impurities can lead to multimodal molecular weight distributions from branching and/or residual MM, high $Đ$ values, and, in extreme cases, cross-linking and gelation.

The desire to avoid MM impurities to access well-defined bottlebrush polymers prepared by ROMP has led to a few recent studies on MM synthesis via direct-growth and growth-then-coupling (Figure 1A, top).[19−21] In one report, Xia and

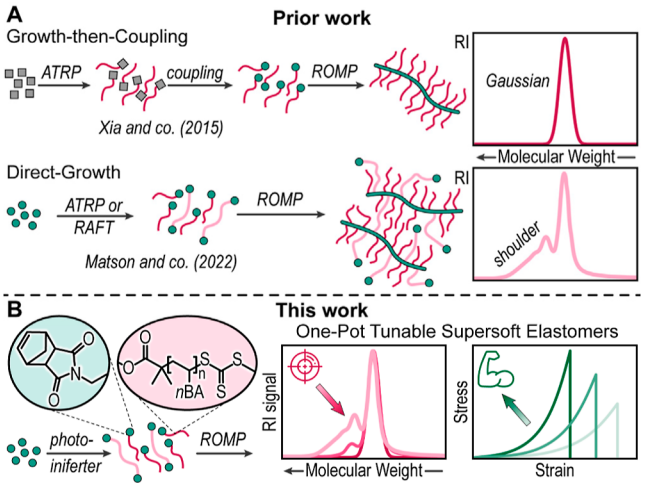

Figure 1. (A) Previous approaches toward MM and bottlebrush synthesis. (B) This work utilizes photoiniferter polymerization to synthesize MMs, followed by ROMP of MMs to yield either bottlebrush polymers with narrow MW distributions or mechanically tunable supersoft bottlebrush networks.

Teo[19] systematically examined different norbornene chain-end-functionalized MMs prepared by controlled radical polymerization, either reversible addition−fragmentation chain transfer (RAFT) polymerization or atom transfer radical polymerization (ATRP). For both controlled radical polymerization methods, a growth-then-coupling strategy was necessary to prepare well-defined ($Đ$ < 1.1) bottlebrush polymers with a maximum degree of polymerization (DP) of 400. Subsequently, Matson and co-workers[20] and Keddie and co-workers[21] independently performed systematic studies on the relationship between monomer type [e.g., styrenic or (meth)-acrylic and (oxa)norbornene] and conversion with the extent of bis-Nb impurity generated for MMs prepared by RAFT polymerization using a direct-growth approach (i.e., norbornene-functionalized chain transfer agent). In both reports, the presence of high-molecular-weight shoulders observed with gel permeation chromatography (GPC) of bottlebrush polymers was ascribed to cross-linking from bis-Nb MM impurity (Figure 1A, bottom). To avoid these shoulders on GPC, it was necessary to lower monomer conversion for the MM syntheses, which was particularly true for *n*-butyl acrylate (*n*BA).[21] Additionally, low DPs for ROMP of the MMs were targeted (=100[20] and 50[18,21]) to further suppress cross-linking (i.e., shoulder formation). Thus, while direct-growth has been demonstrated as a viable strategy toward well-defined bottlebrushes via ROMP, opportunities remain to improve MM purity and, correspondingly, the maximum attainable DP, especially for challenging monomers such as *n*BA that is widely applied in adhesives.

Herein, we demonstrate the optimization and utility of photoiniferter polymerization to synthesize norbornene-functionalized poly(*n*BA) MMs and bottlebrush polymers via ROMP therefrom (Figure 1B). The influence of various parameters (e.g., *n*BA conversion, target ROMP DP, MM molecular weight, and MM concentration) on the formation of bis-Nb MM impurities was systematically characterized using GPC, shear rheology, and tensile testing. Furthermore, using a simple, scalable, and reproducible one-pot approach, MMs containing different "impurity" contents were leveraged to prepare desirable materials, from ultrahigh-molecular-weight bottlebrush polymers (∼1000 kDa) to supersoft elastomers (e.g., moduli ≲100 kPa).

RESULTS AND DISCUSSION

Macromonomers. To ultimately create soft bottlebrush elastomers, *n*BA was selected as the monomer for MM synthesis owing to the low T_g (−55 °C) of poly(*n*BA). Photoiniferter polymerization was selected over traditional RAFT polymerization owing to the dual reactivity of the chain transfer agent (CTA) that acts also as an initiator upon exposure to light. This dual reactivity mitigates the requirement for a supplemental radical initiator that has the potential to generate unfunctionalized chains (i.e., lacking norbornene). Furthermore, photoiniferter polymerization is accomplished without additional catalyst (as needed in ATRP) and at room temperature, which can facilitate thermodynamically favored propagation, minimizing undesirable bimolecular termination events and incorporation of norbornene into the polymer backbone.

Exo-norbornene imide alcohol (**Nb-OH**) was synthesized from the corresponding anhydride and 6-aminohexan-1-ol, followed by coupling with a carboxylic acid-functionalized trithiocarbonate (**CTA**), which was selected for its compatibility with *n*BA (Figure 2A). The resulting norbornene-functionalized iniferter (**Nb-CTA**) was used to prepare a range of MMs via *n*BA homopolymerization in dimethyl sulfoxide (2.87 v/v, 5.2 M *n*BA) with a blue LED (∼470 nm, ∼10 mW/cm^2) (Figure 2B). This polymerization resulted in the controlled formation of norbornene-functionalized poly(*n*-butyl acrylate) (Nb−P*n*BA) having small MM molecular weight distributions ($Đ_{MM}$ ≤ 1.1), as characterized by GPC relative to polystyrene standards (Figure 2C,D). To examine

https://doi.org/10.1021/acs.macromol.4c01419
Macromolecules 2024, 57, 6522−6530

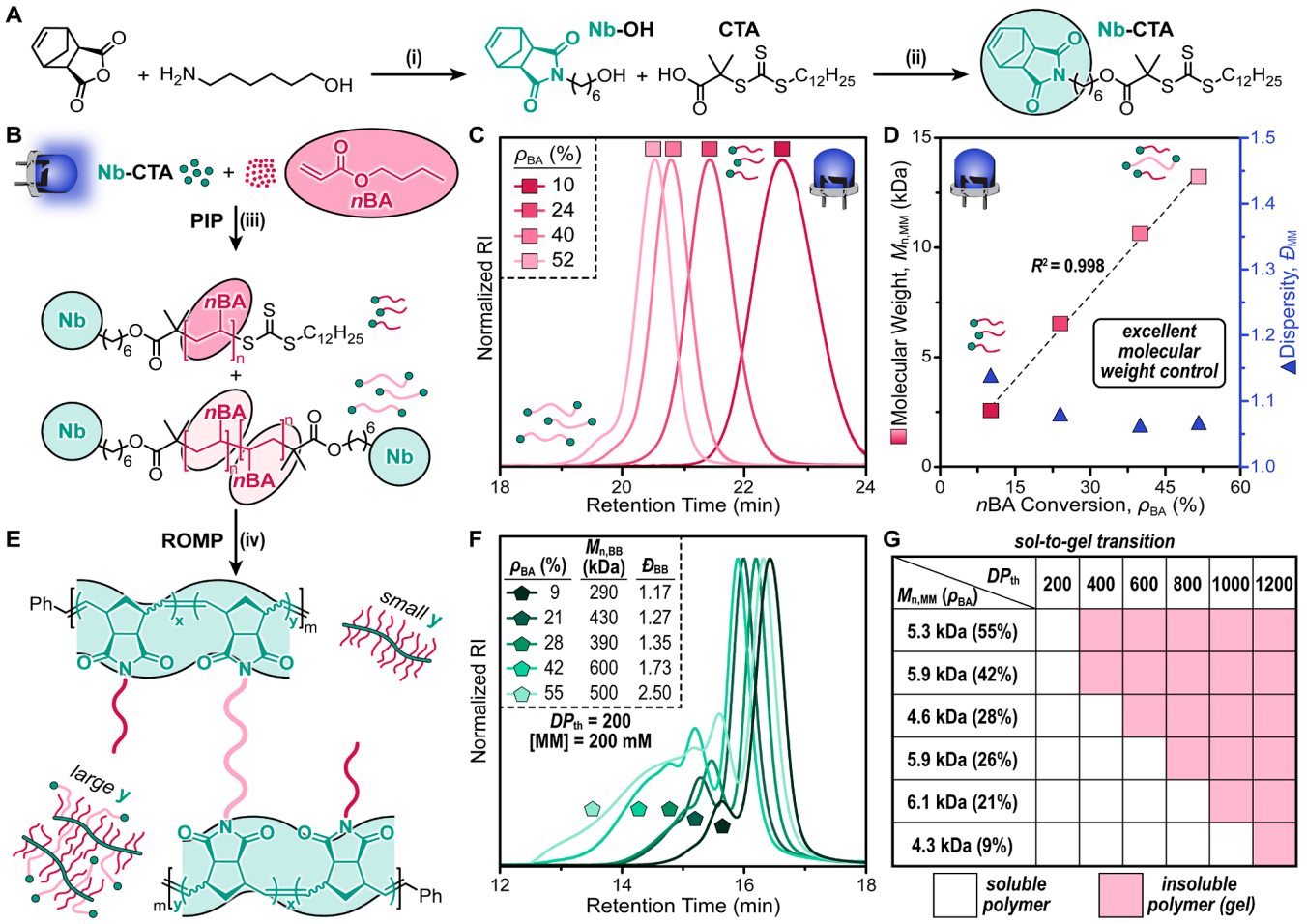

Figure 2. (A) Synthesis of *exo*-norbornene (Nb)-functionalized CTA. (i) Et_3N, toluene, 140 °C, ~12 h, 96% yield; (ii) *N*,*N*′-dicyclohexylcarbodiimide, 4-dimethylaminopyridine, CH_2Cl_2, ~25 °C, ~12 h, 64% yield. (B) Photoiniferter polymerization with Nb-CTA and *n*-butyl acrylate (*n*BA) to generate MM with illustrations of Nb and bis-Nb MM. Note that branching is also hypothesized to occur and contribute to shoulders observed in GPC traces, yet the corresponding illustrations were not included for brevity. (iii) Dimethyl sulfoxide (2.87 v/v, 5.2 M *n*BA), blue LED (~470 nm, ~10 mW/cm^2), ~25 °C, variable exposure times (~1.5−6 h). (C) Representative GPC traces of MMs prepared with different irradiation times and thus different butyl acrylate conversions (ρ_{BA}). (D) Plot of number-average molecular weight ($M_{n,MM}$) and dispersity ($Đ_{MM}$) vs ρ_{BA}. (E) ROMP of MMs with illustrations showing the influence of bis-Nb on bottlebrush coupling. (iv) Modified third generation Grubbs catalyst (G3′), CH_2Cl_2, 15 min, then ethyl vinyl ether (excess). (F) Representative GPC traces for bottlebrushes prepared with a target DP of 200 (50 wt % MM concentration) using MMs prepared with different ρ_{BA}. (G) Vial inversion tests to qualitatively determine gelation for a range of MMs ($M_{n,MM}$ and ρ_{BA}) and theoretical degrees of polymerization (DP_{th}).

the influence of *n*BA conversion (ρ_{BA}) on bottlebrush properties, MMs were synthesized with ρ_{BA} varying from 9 to 55%, while attempting to hold number-average molecular weights constant ($M_{n,MM} \approx 5-6$ kDa) (Figure S3). Notably, high-molecular-weight shoulders were observed, albeit small, when ρ_{BA} exceeded ~40%. These shoulders were attributed to a combination of Nb incorporation into the main-chain resulting in a "branched" polymer structure[21] and bimolecular chain-end termination resulting in bis-Nb MMs. ^{1}H NMR spectroscopy was used to assess the extent of Nb consumption and termination by combination (Figure S4 and Table S1). Monitoring the disappearance of the Nb alkene signal (6.27−6.28 ppm, 2H) during photoiniferter polymerization relative to the terminal methyl of *n*BA (0.91−0.95 ppm, 3H) revealed that going from ~10 to 50% ρ_{BA} increased the Nb incorporation from <1 to ~5%. Similarly, characterizing pure MMs by taking the ratio of the Nb alkene signal to the chain-end methine α to the CTA (4.79−4.85 ppm, 1H) provided estimates for the bis-Nb MM content: <1 to ~9% for samples prepared at a ρ_{BA} of ~10 to 50%, respectively (Figure S5 and Table S1). Notably, altering light intensity, monomer concentration, and choice of solvent for photoiniferter polymerization had little effect on the extent of bis-Nb formation (Figures S7−S9), and thus ρ_{BA} remained as the main variable for MM synthesis in how it influenced bottlebrush polymer architecture and rheological and mechanical properties (Figures S10−S11).

Bottlebrush Polymers. Using a direct-growth ROMP approach, bottlebrush polymers were prepared from the Nb-functionalized MMs. Given the sensitivity of bottlebrush synthesis on MM purity, we chose to initially examine the influence of ρ_{BA} on bottlebrush dispersity ($Đ_{BB}$). The effect was anticipated to be particularly pronounced for the case of *n*BA given its tendency for side reactions during controlled radical polymerizations (i.e., Nb incorporation and termination by combination and disproportionation).[19,25,27] Using a modified third-generation Grubbs catalyst (G3′) that contains pyridyl ligands, ROMP was conducted in dichloromethane, maintaining a constant initial ratio of [MM]/[G3′] = 200 and a fixed initial MM concentration ([MM]) of 200 mM (Figure

https://doi.org/10.1021/acs.macromol.4c01419
Macromolecules 2024, 57, 6522−6530

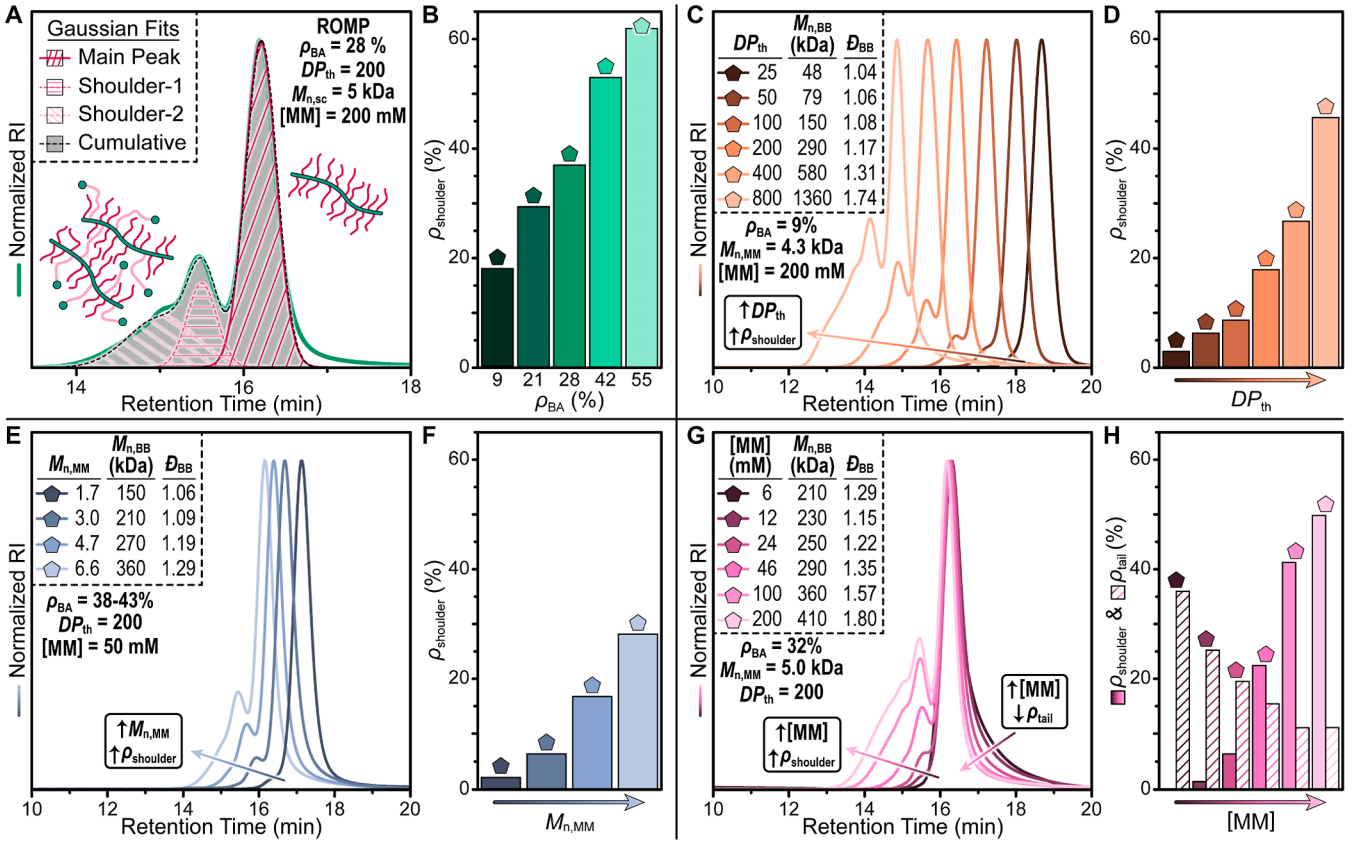

Figure 3. Bottlebrush polymer molecular weight and architecture characterization. (A) Representative GPC trace (RI detection) and corresponding Gaussian fits to determine the percent shoulder contribution ($\rho_{shoulder}$) from branching. (B) Correlation between $\rho_{shoulder}$ and MM ρ_{BA}. (C) GPC traces showing the shoulder evolution as target DP is increased and (D) corresponding $\rho_{shoulder}$ while holding—constant ρ_{BA}, MM number-average molecular weight ($M_{n,MM}$), and MM concentration ([MM]). (E) GPC traces showing the shoulder evolution as $M_{n,MM}$ is increased and (F) corresponding $\rho_{shoulder}$ while holding—constant ρ_{BA}, target DP, and [MM]. (G) GPC traces showing the shoulder evolution as MM concentration is increased and (H) corresponding $\rho_{shoulder}$ and percent of low-molecular-weight tailing (ρ_{tail}) while holding—constant ρ_{BA}, target DP, and $M_{n,MM}$.

2E). Polymerizations were performed at room temperature under a nitrogen atmosphere for 15 min, and then quenched with an excess amount of ethyl vinyl ether (>100 equiv relative to G3′).

All MMs reached near-quantitative conversion (>98.5%) during ROMP, as characterized using GPC via integration of the refractive index (RI) signals for the bottlebrush polymers and remaining MM, while also confirming the viability of this method with ^{1}H NMR spectroscopy (Table S2). Notably, high-molecular-weight shoulders were present in the bottlebrush polymer GPC traces (Figure 2F), which were ascribed to coupling between bottlebrush chains through bis-Nb MMs. Furthermore, as ρ_{BA} increased, so did the size of the shoulder, which agreed with the prior finding that the proportion of bis-Nb species in MM samples increased together with ρ_{BA} (Table S2). Ultimately, bottlebrush samples prepared using MMs with ρ_{BA} values of ∼10−50% provided $M_{n,BB}$ values of ∼290 and 500 kDa and $Đ_{BB}$ values of 1.17 and 2.50, as determined using GPC relative to polystyrene standards. Notably, theoretical $M_{n,BB}$ values were ∼850−1200 kDa (depending on the exact $M_{n,MM}$). However, an underestimation of molecular weight by GPC using linear polymer standards was expected given the significantly higher density of the bottlebrush polymers. Absolute molecular weight characterization by light scattering confirmed that the experimental $M_{n,BB}$ matched theoretical $M_{n,}$ in accordance with a controlled polymerization (ROMP) run to near quantitative conversion (Figures S14−S15 and Tables S4−S5).

As the bis-Nb-to-MM ratio increased, so did the high molecular shoulders in the corresponding bottlebrush GPC traces, and it was predicted that high enough ratios would cause gelation during ROMP. It was also anticipated that as the target DP increased, the effects would become more pronounced given the larger incorporation of bis-Nb units into each bottlebrush main chain. To determine the threshold DP for gelation via ROMP as a function of MM ρ_{BA}, we performed a series of qualitative vial inversion and dissolution tests and quantitative rheological experiments (Figure 2G). ROMP was performed under concentrated conditions (50 wt % MM in CH_2Cl_2) to facilitate high gel fractions upon reaching threshold DP (gel fractions discussed later). Using similar $M_{n,MM}$ values (∼5−6 kDa), varied ρ_{BA} values of 9, 21, 26, 28, 42, and 55% were used for ROMP with [MM]/[G3′] ratios (i.e., target DP) ranging from 200 to 1200. The bottlebrush polymers were synthesized directly in vials and qualitatively analyzed for flow via vial inversion tests, followed by addition of excess CH_2Cl_2 to determine whether the samples dissolved or simply swelled, with the latter indicative of gel formation. Moreover, the bottlebrush networks were characterized via rheology after removing CH_2Cl_2 and swelling with anisole (50 wt %) to mitigate evaporation and physical interactions (e.g., entanglements) that would convolute the

https://doi.org/10.1021/acs.macromol.4c01419
Macromolecules 2024, 57, 6522−6530

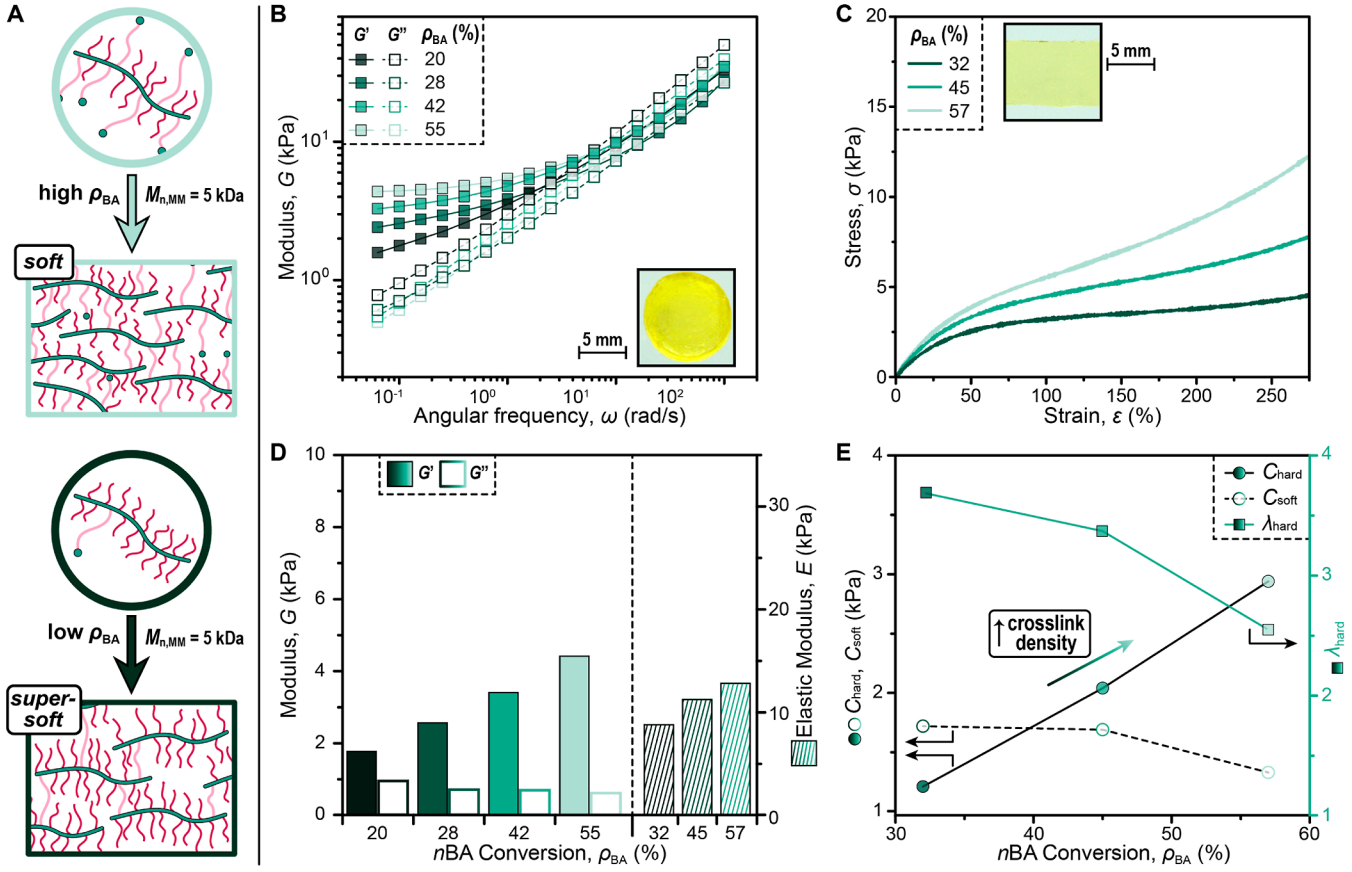

Figure 4. Bottlebrush polymer network mechanical property characterization as a function of ρ_{BA}. (A) Schematic illustration of the MM ρ_{BA} effect on network architecture and mechanical properties ($M_{n,MM}$ = 5 kDa). (B) Rheological shear and (C) uniaxial tensile testing of networks synthesized from MMs with varied ρ_{BA}, along with (D) a bar graph summarizing the data. Photograph insets are representative samples used for characterization. (E) Plot of reduced modulus, C_{hard} and C_{soft}, and onset of strain stiffening, λ_{hard} as a function of ρ_{BA}.

analysis. Samples showing storage moduli (G') greater than loss moduli (G'') were deemed as gels. Notably, the threshold DP for gelation tracked inversely with ρ_{BA}. Decreasing ρ_{BA} for MMs from 55 to 9% resulted in a dramatic increase in threshold DP from 400 to 1200 (Figure 2G). This result agrees with the observation that more bis-Nb forms for MMs prepared at a higher ρ_{BA} and provides a tunable handle to design bottlebrush polymer networks.

Next, Gaussian fits of bottlebrush polymer GPC RI traces below the threshold DP were examined to quantify the amount of coupling that occurred (Figure 3). As a representative example, ROMP of a MM having a ρ_{BA} of 28% resulted in the formation of a bottlebrush having three distinct peaks, where the two shoulders were attributed to structures having two or three bottlebrush polymers coupled together, leading to a ∼2−3× increase in molecular weight (Figure 3A). Fitting all three peaks with individual Gaussians and taking the ratio of shoulder area (sum) over the total area provided an estimate for the percent of branching, $\rho_{shoulder}$ (Figure 3B). In performing this analysis, a clear trend emerged where increasing ρ_{BA} led to an increase in $\rho_{shoulder}$. Specifically, ρ_{BA} values of 9, 21, 28, 42, and 55% corresponded to $\rho_{shoulder}$ values of 18, 29, 37, 53, and 62%. Thus, the predominant bottlebrush species was the pure linear structure when ρ_{BA} was <30%. The statistical significance of this relationship between ρ_{BA} and $\rho_{shoulder}$ was further supported by a Pearson correlation coefficient[29] of 0.994, as values >0.8 indicates a strong correlation (Table S6).

To expand upon our understanding of the factors that influence bottlebrush architectures beyond ρ_{BA}, we performed a systematic series of ROMPs varying instead target DP (Figure 3C,D), $M_{n,MM}$ (Figure 3E,F), and [MM] (Figure 3G,H). In each case, GPC analysis relative to polystyrene standards was used to evaluate the molecular weight, $Đ_{BB}$, and $\rho_{shoulder}$. Initially, the influence on target DP was examined using a MM produced with a low ρ_{BA} of 9% to minimize cross-linking. Additionally, $M_{n,MM}$ (4.3 kDa), [MM] (∼200 mM), and MM ROMP conversion (>98%) were held constant. Under these conditions, the $M_{n,BB}$ (and $Đ_{BB}$) values were 48 kDa (1.04), 79 kDa (1.06), 150 kDa (1.08), 290 kDa (1.17), 580 kDa (1.31), and 1360 kDa (1.74) for target DP values of 25, 50, 100, 200, 400, and 800, respectively (Figure 3C). As expected, $\rho_{shoulder}$ values increased as DP increased: 3, 6, 9, 18, 27, and 56%, respectively (Figure 3D), providing a Pearson correlation coefficient of 0.993 (Table S6). From these experiments, well-defined bottlebrush polymers ($Đ_{BB}$ < 1.2) were achieved for samples with a target DP up to 200, corresponding to a theoretical $M_{n,BB}$ of 860 kDa.

The influence of $M_{n,MM}$ was examined next, holding constant ρ_{BA} (38−43%), target DP (200), [MM] (50 mM), and MM ROMP conversion (>98%). Under these conditions, $M_{n,BB}$ (and $Đ_{BB}$) values were 150 kDa (1.06), 210 kDa (1.09), 270 kDa (1.19), and 360 kDa (1.29) for $M_{n,MM}$ values of 1.7, 3.0, 4.7, and 6.6 kDa, respectively (Figure 3E). Furthermore, increasing $M_{n,MM}$ resulted in an increase in $\rho_{shoulder}$: 2, 6, 17, and 28%, respectively, corresponding to a Pearson correlation

https://doi.org/10.1021/acs.macromol.4c01419
Macromolecules 2024, 57, 6522−6530

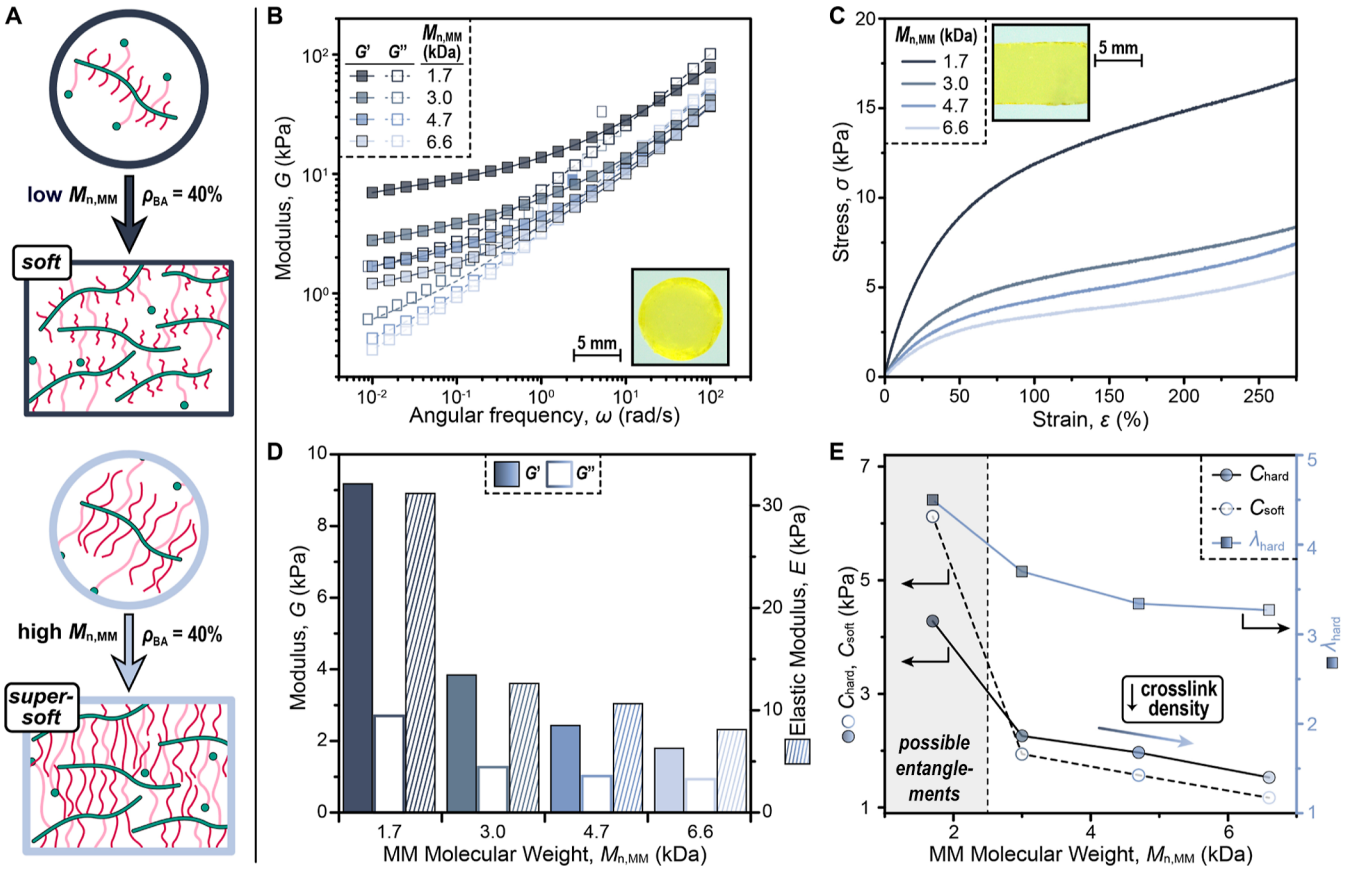

Figure 5. Bottlebrush polymer network mechanical property characterization as a function of $M_{n,MM}$. (A) Schematic illustration of the $M_{n,MM}$ effect on network architecture and mechanical properties (ρ_{BA} = 40%). (B) Rheological shear and (C) uniaxial tensile testing of networks synthesized from MMs with varied $M_{n,MM}$, along with (D) a bar graph summarizing the data. Photograph insets are representative samples used for characterization. (E) Plot of reduced modulus, C_{hard} and C_{soft}, and onset of strain stiffening, λ_{hard} as a function of $M_{n,MM}$.

coefficient of 0.898 (Table S6). From these results, the effect of $M_{n,MM}$ on $\rho_{shoulder}$ was less pronounced than varying DP, but it similarly indicated that despite having very similar ρ_{BA} values (~40%) for photoiniferter polymerization of MMs, longer MM polymer chains were more prone to side reactions (e.g., combination to form bis-Nb) relative to smaller analogues (Figure 3F).

As a final effect, the influence of ROMP [MM] was examined, holding constant ρ_{BA} (32%), target DP (200), $M_{n,MM}$ (5 kDa), and MM ROMP conversion (>98%). The $M_{n,BB}$ (and $Đ_{BB}$) values that resulted were 210 kDa (1.29), 230 kDa (1.15), 250 kDa (1.22), 290 kDa (1.35), 360 kDa (1.57), and 410 kDa (1.80) for MM concentrations of 6, 12, 24, 45, 100, and 200 mM, respectively (Figure 3G). Notably, the nonmonotonic change in $Đ_{BB}$ upon changing [MM] arose from a trade-off between high-molecular-weight shoulders and low-molecular-weight tails. Specifically, increasing [MM] for ROMP resulted in an increase in $\rho_{shoulder}$ values: <0.1, 1, 6, 22, 41, and 50%, respectively, with a Pearson correlation coefficient of 0.978 (Table S6). In contrast, increasing [MM] led to a decrease in ρ_{tail} values: 36, 25, 20, 15, 11, and 11%, respectively. For low [MM] cases, we hypothesized that tailing occured from premature chain termination and/or cross metathesis that becomes more prevalent as the kinetics of ROMP decreases and polymer diffusion increases. Monitoring conversion as a function of time for ROMPs with varied initial [MM]'s confirmed that polymerization kinetics decrease together with concentration (Figure S15) and supported the hypothesis that competitive chain termination may have occured and accounted for the observed tailing.[30] Simultaneously, the decrease in $\rho_{shoulder}$ upon decreasing [MM] was postulated to arise from an increased likelihood that active chain-ends interacted with residual MM as opposed to constrained pendent Nb side chains at high MM conversion (>95%). Thus, an ideal concentration can be selected to minimize $\rho_{shoulder}$ and/or ρ_{tail}. In the present case, a [MM] of ~25 mM appeared to provide a good balance between the two, as reflected in the relatively small $Đ_{BB}$ value of ~1.2 for a theoretical $M_{n,BB}$ of ~1000 kDa, which to the best of our knowledge is unprecedented for brush polymers containing acrylate-based arms.

Bottlebrush Polymer Networks. Given their potential utility as supersoft materials for biomedical applications, bottlebrush polymer networks (elastomers) were created by leveraging the intrinsic bis-Nb species present in our MMs. Furthermore, it was envisioned that cross-link density and concomitant mechanical properties could be easily and reliably tuned by varying ρ_{BA} and $M_{n,MM}$ (Figures 4 and 5). To facilitate gelation, ROMPs were performed using a high [MM] (50 wt % ≈ 200 mM for $M_{n,MM}$ of ~5 kDa) together with a high target DP ([MM]/[G3′] = 2000). Within ~15 s of G3′ addition into the MM solution, the reaction became viscous, and within ~2 min, it turned into a gel. To ensure high MM conversion, samples were left to react for 1 h. Thorough washing to remove unreacted MM and bis-Nb cross-linker was accomplished by swelling the gels in additional CH_2Cl_2 and

https://doi.org/10.1021/acs.macromol.4c01419
Macromolecules 2024, 57, 6522−6530

replacing the solvent every ∼12 h, 3 ×. Subsequently, the gels were dried under reduced pressure and weighed to determine gel fractions prior to mechanical testing. Notably, high gel fractions ranging from 92 to 98% were determined using this gravimetric analysis, which suggests that a high MM conversion was reached (Table S7).

To examine the influence of ρ_{BA} on mechanical properties, four different bottlebrush networks were synthesized holding constant $M_{n,MM}$ of ∼5 kDa (Figure 4A). Using MMs with ρ_{BA} values of 55, 42, 28, and 20%, samples were prepared, and their linear viscoelastic properties were probed using linear amplitude oscillatory shear rheology (Figure 4B). Frequency sweeps were conducted from 0.01 to 100 rad/s within the linear viscoelastic regime (i.e., at a strain of 10%) at room temperature. Notably, the storage modulus, G', at a frequency of 0.1 rad/s increased from 1.8 to 4.4 kPa as the conversion of *n*-butyl acrylate during photoiniferter polymerization (ρ_{BA}) increased from 20 to 55%, revealing that MMs synthesized to higher ρ_{BA} during photoiniferter polymerization afford more solid-like networks, consistent with the presence of higher fractions of cross-linker in the ROMP polymerization. Moreover, the storage and loss moduli illustrate that the networks are soft, viscoelastic, and weakly cross-linked.[31]

The stress−strain curves under uniaxial tension validated the rheological observations. Specimens were elongated up to a strain of $\varepsilon \approx 300\%$—the physical limit of the dynamic mechanical analyzer (DMA)—at an initial strain rate of 0.005 s^{-1}. MMs with ρ_{BA} values of 57, 45, and 32% resulted in supersoft bottlebrush networks with elastic moduli (E) values of 12.8, 11.2, and 8.8 kPa, respectively (Figure 4C). These moduli were approximately equal to three times the storage modulus, G', at 0.1 rad/s, consistent with the incompressibility of the networks (i.e., Poisson ratio, $\nu \approx 0.5$). These results agree with the prior finding that MMs prepared at lower ρ_{BA} contain less bis-Nb cross-linker and thus should result in bottlebrush networks with lower cross-link density and correspondingly smaller G' and E values (Figure 4D). Notably a Pearson correlation coefficient of 0.99 between ρ_{BA} and G' or E indicates that these values are strongly correlated (Table S6).

At moderate-to-large deformations, the bottlebrush networks first strain softened and then strain stiffened (Figures 4C and S17). This behavior is similar to that of weakly cross-linked linear networks and consistent with the complex moduli measured in linear amplitude oscillatory shear (i.e., G' at 1 rad/s < 0.1 MPa, tan δ at 1 rad/s > 0.3). To rationalize this behavior, a Mooney plot[31] was generated, where the renormalized stress $f^* = \sigma/(\lambda - \lambda^{-2})$ was evaluated as a function of the reciprocal strain λ^{-1} (Figure S18 and eq S2). In this plot, the Mooney stress is constant for Neo-Hookean networks (i.e., ideal rubbers), and any dependence of f^* on λ^{-1} can be interpreted as a signature of entanglements, viscoelastic relaxation, and finite extensibility of the polymer chains.[31] Using the minimum in f^*, one can define three material parameters: (i) a reduced modulus, C_{hard}, stemming from chemical cross-links, (ii) a reduced modulus, $C_{soft} = E/3 - C_{hard}$, arising from entanglements and/or viscoelastic chain relaxation, and (iii) an onset of strain stiffening, λ_{hard}, resulting from the finite extensibility of the network chains. Given that bottlebrush polymers have high entanglement molecular weights,[3] viscoelastic chain relaxation (e.g., arm retraction) or "flow" was postulated to be the major mechanism responsible for C_{soft} (and the dependence of G' on frequency). Plotting these parameters as a function of ρ_{BA} revealed that increasing ρ_{BA} resulted in bottlebrush networks that were stiffer and less extensible, consistent with the increased fraction of bis-Nb cross-linker in MMs. Specifically, as ρ_{BA} increased from 32 to 57%, C_{hard} increased from 1.2 to 2.9 kPa and λ_{hard} decreased from 3.7 to 2.6 (Figure 4E). This observation indicates that the networks become more cross-linked as ρ_{BA} increases. Additionally, C_{soft} decreased from 1.7 to 1.3 kPa, indicating that the constituent chains are slightly less resistant to sliding.

As a final study, the influence of bottlebrush side-chain length (i.e., $M_{n,MM}$) on mechanical properties was examined while holding constant ρ_{BA} at ∼40% (Figure 5A). Four different bottlebrush networks were synthesized with varying $M_{n,MM}$ values of 1.7, 3.0, 4.7, and 6.6 kDa. Rheological characterization unveiled a clear trend, where increasing $M_{n,MM}$ from 1.7 to 6.6 kDa corresponded to a ∼5× decrease in G', from 9.2 to 1.8 kPa at a frequency of 0.1 rad/s (Figure 5B). Correspondingly, as $M_{n,MM}$ increased, E values from tensile testing decreased: 31.2, 12.6, 10.6, and 8.1 kPa, respectively (Figure 5C). These results were postulated to arise from a decrease in cross-link density as the side-chain length increased, resulting in reduced stiffness (Figure 5D). Notably a Pearson correlation coefficient of 0.99 between $M_{n,MM}$ and G' or E indicates that these values are strongly correlated (Table S6).

Insights into the structure−property relationships were gained by inspecting the influence of $M_{n,MM}$ on C_{hard}, C_{soft}, and λ_{hard} (Figure 5E). First, the decrease in C_{hard} and λ_{hard} at high $M_{n,MM}$ indicated that the networks become less cross-linked. This observation agrees with the photoiniferter polymerizations having the same molar fraction of bis-Nb cross-linker, yet reduced bis-NB molarity as $M_{n,MM}$ increases. Second, the sharp increase in C_{hard} and C_{soft} at $M_{n,MM}$ < 3.0 kDa suggested that the bottlebrush networks might entangle with these shorter side chains. This is further supported by $C_{soft} > C_{hard}$ at $M_{n,MM}$ = 1.7 kDa, as well as hysteresis under step cyclic loading (Figures 5E and S19B). These results indicate that $M_{n,MM}$ can be leveraged to concurrently adjust cross-link density and entanglements of bottlebrush networks to tune their bulk mechanical properties (e.g., strain stiffening).

CONCLUSIONS

Direct-growth photoiniferter polymerizations of *n*-butyl acrylate (*n*BA) from norbornene-functionalized CTAs were used to synthesize MMs that were subsequently employed in ROMP to access bottlebrush polymers with tunable molecular weight, architecture, and mechanical properties. A systematic examination of bis-norbornenyl (bis-Nb) species formed during the photoiniferter polymerization process revealed that higher *n*BA conversion (ρ_{BA}) resulted in more bis-Nb, which led to a lower ROMP DP threshold for bottlebrush gelation. Additionally, optimization of ROMP was accomplished by varying target DP, $M_{n,MM}$, and [MM] concentration, enabling the preparation of ultrahigh-molecular-weight bottlebrush polymers (∼1000 kDa) with a narrow-molecular-weight distribution ($Đ \approx 1.2$). Provided the good control over bis-Nb content through varying ρ_{BA}, supersoft bottlebrush networks (<100 kPa) with high gel fractions (>90%) were prepared directly from MMs without requiring a separate synthesis and addition of cross-linkers. In this manner, elastomers (solvent-free) with tunable supersoft moduli, strain softening, and strain hardening were accessible. In turn, these and/or related materials may find applications in the biomedical arena, such as

https://doi.org/10.1021/acs.macromol.4c01419
Macromolecules 2024, 57, 6522−6530

scaffolds for regenerative medicine and pressure-sensitive adhesives that interface favorably with the human body.

■ ASSOCIATED CONTENT

Supporting Information

The Supporting Information is available free of charge at https://pubs.acs.org/doi/10.1021/acs.macromol.4c01419.

Materials, methods, instrumentation, MM synthesis via photoiniferter polymerization, bottlebrush synthesis via ROMP, MM optimization via photoiniferter polymerization, MM optimization and gelation via rheology, MM optimization and kinetic study, gel fraction, mechanical properties of bottlebrush gels, and ^{1}H and ^{13}C NMR and mass spectra (PDF)

■ AUTHOR INFORMATION

Corresponding Authors

Gabriel E. Sanoja − *McKetta Department of Chemical Engineering, The University of Texas at Austin, Austin, Texas 78712, United States;* orcid.org/0000-0001-5477-2346; Email: gesanoja@che.utexas.edu

Zachariah A. Page − *Department of Chemistry, The University of Texas at Austin, Austin, Texas 78712, United States;* orcid.org/0000-0002-1013-5422; Email: zpage@utexas.edu

Authors

Yutong Liu − *Department of Chemistry, The University of Texas at Austin, Austin, Texas 78712, United States*

Henry L. Cater − *Department of Chemistry, The University of Texas at Austin, Austin, Texas 78712, United States*

Anthony J. Arrowood − *McKetta Department of Chemical Engineering, The University of Texas at Austin, Austin, Texas 78712, United States*

Complete contact information is available at: https://pubs.acs.org/10.1021/acs.macromol.4c01419

Author Contributions

Conceptualization (**YL** and **ZAP**); methodology (**YL**, **HLC**, **AJA**, **GES**, and **ZAP**); investigation (**YL**, **HLC**, and **AJA**); visualization (**YL** and **ZAP**); funding acquisition (**GES** and **ZAP**); project administration (**GES** and **ZAP**); supervision (**GES** and **ZAP**); writing—original draft (**YL**); writing—review and editing (**YL**, **HLC**, **AJA**, **GES**, and **ZAP**).

Notes

The authors declare no competing financial interest.

■ ACKNOWLEDGMENTS

The authors acknowledge primary support from the National Science Foundation under Grant no. DMR-2045336 (Y.L., H.L.C., and Z.A.P.). Partial support was provided by the Robert A. Welch Foundation under Grant no. F-2007 (Z.A.P.), the Camille and Henry Dreyfus Foundation under Award no. TC-23-059 (Z.A.P.; partial materials and supplies support), and the Cockrell School of Engineering (A.J.A. and G.E.S.).

■ ABBREVIATIONS

ROMP, ring-opening metathesis polymerization; MM, macromonomer; $Đ$, dispersity; Nb, norbornene; GPC, gel permeation chromatography; *n*BA, *n*-butyl acrylate; ρ_{BA}, conversion of *n*BA during MM synthesis; M_n, MM, number-average molecular weight of MM; M_n, BB, number-average molecular weight of bottlebrush; DP, degree of polymerization; DP_{th}, theoretical degree of polymerization; $\rho_{shoulder}$, fraction of GPC trace fit to the high-molecular-weight shoulder; ρ_{tail}, fraction of GPC trace fit to the low-molecular-weight tail; G', storage modulus; G'', loss modulus; E, elastic tensile modulus; σ, tensile stress; ε, tensile strain percent; f^*, renormalized stress; ν, Poisson ratio; C, reduced modulus; λ^{-1}, reciprocal strain

■ REFERENCES

(1) Sheiko, S. S.; Sumerlin, B. S.; Matyjaszewski, K. Cylindrical Molecular Brushes: Synthesis, Characterization, and Properties. *Prog. Polym. Sci.* **2008**, *33* (7), 759−785.

(2) Zhang, M.; Müller, A. H. E. Cylindrical Polymer Brushes. *J. Polym. Sci., Part A: Polym. Chem.* **2005**, *43* (16), 3461−3481.

(3) Daniel, W. F. M.; Burdyńska, J.; Vatankhah-Varnoosfaderani, M.; Matyjaszewski, K.; Paturej, J.; Rubinstein, M.; Dobrynin, A. V.; Sheiko, S. S. Solvent-Free, Supersoft and Superelastic Bottlebrush Melts and Networks. *Nat. Mater.* **2016**, *15* (2), 183−189.

(4) Cai, L.-H.; Kodger, T. E.; Guerra, R. E.; Pegoraro, A. F.; Rubinstein, M.; Weitz, D. A.; Cai, L.; Kodger, T. E.; Guerra, R. E.; Pegoraro, A. F.; Weitz John A Paulson, D. A.; Rubinstein, M. Soft Poly(Dimethylsiloxane) Elastomers from Architecture-Driven Entanglement Free Design. *Adv. Mater.* **2015**, *27* (35), 5132−5140.

(5) Sarapas, J. M.; Chan, E. P.; Rettner, E. M.; Beers, K. L. Compressing and Swelling To Study the Structure of Extremely Soft Bottlebrush Networks Prepared by ROMP. *Macromolecules* **2018**, *51* (6), 2359−2366.

(6) Miyake, G. M.; Weitekamp, R. A.; Piunova, V. A.; Grubbs, R. H. Synthesis of Isocyanate-Based Brush Block Copolymers and Their Rapid Self-Assembly to Infrared-Reflecting Photonic Crystals. *J. Am. Chem. Soc.* **2012**, *134* (34), 14249−14254.

(7) Sveinbjörnsson, B. R.; Weitekamp, R. A.; Miyake, G. M.; Xia, Y.; Atwater, H. A.; Grubbs, R. H. Rapid Self-Assembly of Brush Block Copolymers to Photonic Crystals. *Proc. Natl. Acad. Sci. U.S.A.* **2012**, *109* (36), 14332−14336.

(8) Sun, G.; Cho, S.; Clark, C.; Verkhoturov, S. V.; Eller, M. J.; Li, A.; Pavía-Jiménez, A.; Schweikert, E. A.; Thackeray, J. W.; Trefonas, P.; Wooley, K. L. Nanoscopic Cylindrical Dual Concentric and Lengthwise Block Brush Terpolymers as Covalent Preassembled High-Resolution and High-Sensitivity Negative-Tone Photoresist Materials. *J. Am. Chem. Soc.* **2013**, *135* (11), 4203−4206.

(9) Maw, M.; Dashtimoghadam, E.; Keith, A. N.; Morgan, B. J.; Tanas, A. K.; Nikitina, E.; Ivanov, D. A.; Vatankhah-Varnosfaderani, M.; Dobrynin, A. V.; Sheiko, S. S. Sticky Architecture: Encoding Pressure Sensitive Adhesion in Polymer Networks. *ACS Cent. Sci.* **2023**, *9* (2), 197−205.

(10) Keith, A. N.; Vatankhah-Varnosfaderani, M.; Clair, C.; Fahimipour, F.; Dashtimoghadam, E.; Lallam, A.; Sztucki, M.; Ivanov, D. A.; Liang, H.; Dobrynin, A. V.; Sheiko, S. S. Bottlebrush Bridge between Soft Gels and Firm Tissues. *ACS Cent. Sci.* **2020**, *6* (3), 413−419.

(11) Sheiko, S. S.; Dobrynin, A. V. Architectural Code for Rubber Elasticity: From Supersoft to Superfirm Materials. *Macromolecules* **2019**, *52* (20), 7531−7546.

(12) Keith, A. N.; Clair, C.; Lallam, A.; Bersenev, E. A.; Ivanov, D. A.; Tian, Y.; Dobrynin, A. V.; Sheiko, S. S. Independently Tuning Elastomer Softness and Firmness by Incorporating Side Chain Mixtures into Bottlebrush Network Strands. *Macromolecules* **2020**, *53* (21), 9306−9312.

(13) Mapas, J. K. D.; Thomay, T.; Cartwright, A. N.; Ilavsky, J.; Rzayev, J. Ultrahigh Molecular Weight Linear Block Copolymers: Rapid Access by Reversible-Deactivation Radical Polymerization and Self-Assembly into Large Domain Nanostructures. *Macromolecules* **2016**, *49* (10), 3733−3738.

(14) Patel, B. B.; Walsh, D. J.; Kim, D. H.; Kwok, J.; Lee, B.; Guironnet, D.; Diao, Y. Tunable Structural Color of Bottlebrush Block Copolymers through Direct-Write 3D Printing from Solution. *Sci. Adv.* **2020**, *6* (24), 7202−7212.

(15) Vatankhah-Varnosfaderani, M.; Keith, A. N.; Cong, Y.; Liang, H.; Rosenthal, M.; Sztucki, M.; Clair, C.; Magonov, S.; Ivanov, D. A.; Dobrynin, A. V.; Sheiko, S. S. Chameleon-like Elastomers with Molecularly Encoded Strain-Adaptive Stiffening and Coloration. *Science* **2018**, *359* (6383), 1509−1513.
(16) Radzinski, S. C.; Foster, J. C.; Matson, J. B. Synthesis of Bottlebrush Polymers via Transfer-to and Grafting-through Approaches Using a RAFT Chain Transfer Agent with a ROMP-Active Z-Group. *Polym. Chem.* **2015**, *6* (31), 5643−5652.
(17) Neary, W. J.; Fultz, B. A.; Kennemur, J. G. Well-Defined and Precision-Grafted Bottlebrush Polypentenamers from Variable Temperature ROMP and ATRP. *ACS Macro Lett.* **2018**, *7* (9), 1080−1086.
(18) Li, Z.; Zhang, K. E.; Ma, J.; Chong, C.; Wooley, K. L. Facile Syntheses of Cylindrical Molecular Brushes by a Sequential RAFT and ROMP "Grafting-Through" Methodology. *J. Polym. Sci., Part A: Polym. Chem.* **2009**, *47* (20), 5557−5563.
(19) Teo, Y. C.; Xia, Y. Importance of Macromonomer Quality in the Ring-Opening Metathesis Polymerization of Macromonomers. *Macromolecules* **2015**, *48* (16), 5656−5662.
(20) Alaboalirat, M.; Vu, C.; Matson, J. B. Radical-Radical Coupling Effects in the Direct-Growth Grafting-through Synthesis of Bottlebrush Polymers Using RAFT and ROMP. *Polym. Chem.* **2022**, *13* (41), 5841−5851.
(21) Naguib, M.; Nixon, K. L.; Keddie, D. J. Effect of Radical Copolymerization of the (Oxa)Norbornene End-Group of RAFT-Prepared Macromonomers on Bottlebrush Copolymer Synthesis via ROMP. *Polym. Chem.* **2022**, *13* (10), 1401−1410.
(22) Li, X.; ShamsiJazeyi, H.; Pesek, S. L.; Agrawal, A.; Hammouda, B.; Verduzco, R. Thermoresponsive PNIPAAM Bottlebrush Polymers with Tailored Side-Chain Length and End-Group Structure. *Soft Matter* **2014**, *10* (12), 2008−2015.
(23) Alaboalirat, M.; Qi, L.; Arrington, K. J.; Qian, S.; Keum, J. K.; Mei, H.; Littrell, K. C.; Sumpter, B. G.; Carrillo, J.-M. Y.; Verduzco, R.; Matson, J. B. Amphiphilic Bottlebrush Block Copolymers: Analysis of Aqueous Self-Assembly by Small-Angle Neutron Scattering and Surface Tension Measurements. *Macromolecules* **2019**, *52* (2), 465−476.
(24) Nam, J.; Kim, Y.; Kim, J. G.; Seo, M. Self-Assembly of Monolayer Vesicles via Backbone-Shiftable Synthesis of Janus Core-Shell Bottlebrush Polymer. *Macromolecules* **2019**, *52* (24), 9484−9494.
(25) Cheng, C.; Khoshdel, E.; Wooley, K. L. ATRP from a Norbornenyl-Functionalized Initiator: Balancing of Complementary Reactivity for the Preparation of α-Norbornenyl Macromonomers/ω-Haloalkyl Macroinitiators. *Macromolecules* **2005**, *38* (23), 9455−9465.
(26) Clarke, B. R.; Tew, G. N. Synthesis and Characterization of Poly(Ethylene Glycol) Bottlebrush Networks via Ring-Opening Metathesis Polymerization. *J. Polym. Sci.* **2022**, *60* (9), 1501−1510.
(27) Patton, D. L.; Advincula, R. C. A Versatile Synthetic Route to Macromonomers via RAFT Polymerization. *Macromolecules* **2006**, *39* (25), 8674−8683.
(28) Onbulak, S.; Rzayev, J. Synthesis and One-Dimensional Assembly of Cylindrical Polymer Nanoparticles Prepared from Tricomponent Bottlebrush Copolymers. *J. Polym. Sci., Part A: Polym. Chem.* **2017**, *55* (23), 3868−3874.
(29) Akoglu, H. User's Guide to Correlation Coefficients. *Turkish J. Emerg. Med.* **2018**, *18* (3), 91−93.
(30) Radzinski, S. C.; Foster, J. C.; Chapleski, R. C.; Troya, D.; Matson, J. B. Bottlebrush Polymer Synthesis by Ring-Opening Metathesis Polymerization: The Significance of the Anchor Group. *J. Am. Chem. Soc.* **2016**, *138* (22), 6998−7004.
(31) Creton, C.; Ciccotti, M. Fracture and Adhesion of Soft Materials: A Review. *Rep. Prog. Phys.* **2016**, *79* (4), 046601.

https://doi.org/10.1021/acs.macromol.4c01419
Macromolecules 2024, 57, 6522−6530